中国激光

温稠密金的太赫兹时域光谱实验

孙旭[1]，吴海忠[1]，王小伟[1]，吕治辉[1]，张栋文[1*]，刘东晓[2]，范伟[2]，粟敬钦[2]，周维民[2]，谷渝秋[2]，赵增秀[1**]，袁建民[1,3***]

[1]国防科技大学理学院，湖南 长沙 410073；
[2]中国工程物理研究院激光聚变研究中心，等离子体物理重点实验室，四川 绵阳 621900；
[3]中国工程物理研究院研究生院，北京 100193

摘要 太赫兹波为高能量密度物质提供了独一无二的诊断手段，但在大型高能量密度装置上实现极端条件下物质状态的太赫兹时域光谱诊断技术仍面临巨大挑战。本文报道了在低重复频率、高能量激光装置上开展的光脉冲泵浦-太赫兹探测实验。利用钛宝石飞秒激光器输出焦耳量级的单发脉冲，单发脉冲经磷酸二氢钾倍频后加热 30 nm 厚自支撑金膜，产生均匀的温稠密金等离子体；同时，将大孔径铌酸锂晶片通过光整流产生的单脉冲能量为 7 μJ 的太赫兹脉冲作为探测光，利用金属阶梯镜实现了单发太赫兹波形探测，获得了温稠密金在太赫兹波段的时间分辨的电导率数据，为检验双温模型中电子-离子耦合系数等关键参数的准确性提供了新基准。

关键词 超快光学；太赫兹时域光谱；单发泵浦-探测；极端物态诊断；电导率

中图分类号 O441.4 **文献标志码** A **DOI**：10.3788/CJL230791

1 引 言

太赫兹（THz，0.1～10 THz）在电磁波谱中介于微波到远红外之间。太赫兹辐射独特的频谱范围使得太赫兹时域光谱技术成为研究气体分子转动[1-2]、液体分子动力学[3-4]、固体晶格振动[5-6]、等离子体振荡[7]等的有力工具。光学泵浦-太赫兹探测作为太赫兹时域光谱应用的重要组成部分，常被用来研究非平衡态的性质，如半导体中的载流子动力学和迁移率[8-9]。超强激光能够产生高能量密度的极端非平衡物理状态，太赫兹时域光谱技术能够诊断这种瞬态物质的电导率等参数[10]。温稠密物质的直流电导率是研究该物质结构、辐射性质和动力学的重要参数，但是在大型高能量密度装置上获取温稠密物质的时间分辨的电导率还面临着巨大挑战。用太赫兹时域光谱技术诊断均匀温稠密物质状态在实验上的挑战主要包含两个方面：一是缺乏强场太赫兹源。温稠密物质是一种与固体具有相同密度的等离子体，太赫兹电场在该物质中的透过率往往在 1% 量级，只有强太赫兹场透过温稠密物质样品后的太赫兹波形才有可能被探测到。二是缺乏单发太赫兹波形探测手段。低重复频率、高脉冲能量的超快激光产生温稠密物质的过程是破坏性的、不可重复的，温稠密物质的信息包含在透射的一个太赫兹脉冲上，因而必须发展单发太赫兹波形探测技术。

目前，强场太赫兹物理研究正处于快速发展期，人们利用强场太赫兹源已经观察到了一大批新颖的实验现象，如太赫兹拓扑开关[11]、紧凑型太赫兹电子加速器和压缩器[12-15]、单发太赫兹生物成像[16]、太赫兹引起的晶体或液体中的非线性效应[17-18]、太赫兹驱动的高次谐波产生（HHG）[19-20]以及对物质瞬态性质的太赫兹操纵[21-23]。我国在大型高能量密度装置上产生了脉冲能量最高的太赫兹脉冲。2019 年，中国科学院物理研究所利用皮秒超强激光装置在固体薄膜靶中加速大量高能电子，当电子从靶背面逃逸到真空时，通过渡越辐射激发了脉冲能量高达 55 mJ 的高强度太赫兹辐射[24]。

在利用飞秒激光脉冲产生单周期、宽频带、强场太赫兹辐射的方法中，光学整流（OR）是一种常用的方案。铌酸锂（$LiNbO_3$，简记为"LN"）具有非线性系数大、损伤阈值高[25]、带隙大（≈4 eV）的特点，采用钛宝石飞秒激光器泵浦时不会受到双光子吸收的影响，而且生长工艺较为成熟，高质量商业化铌酸锂晶片直径能达到 152 mm[26]。因此，铌酸锂是产生强太赫兹的一种重要材料。铌酸锂晶体中激光脉冲的群速度远大于太赫兹波的相速度，因此常采用倾斜波前技术来实现相位匹配[27-31]。最近，北京航空航天大学分别利用脉冲能量为 214 mJ 和 1.2 J 的钛宝石激光器泵浦低温冷

收稿日期：2023-05-04；**修回日期**：2023-06-02；**录用日期**：2023-06-19；**网络首发日期**：2023-07-06

基金项目：国家重点研发计划（2019YFA0307703）、国家自然科学基金重点项目（12234020）、国家自然科学基金（12175211，11974425，11974426）

通信作者：*dwzhang@nudt.edu.cn；**zhaozengxiu@nudt.edu.cn；***jmyuan@gscaep.ac.cn

却的铌酸锂棱镜，产生了 1.4 mJ 和 13.9 mJ 的太赫兹脉冲[32-33]。倾斜波前相位匹配要求铌酸锂棱镜的切割角度在 63°左右，导致太赫兹与泵浦光束非共线传播[34]。在低重复频率、高能量激光装置上开展光学泵浦-太赫兹探测研究时，太赫兹与泵浦光束的非共线传播将会为光路排布带来巨大的技术挑战。用大激光装置输出的激光脉冲直接泵浦大口径铌酸锂晶片，然后通过光整流获得与泵浦激光共线传播的强太赫兹脉冲也是一种实际可行的方案[26]。

传统的太赫兹波形探测技术利用多个太赫兹脉冲重复扫描采样，如电光采样探测[35]、基于空气等离子体电压偏置的相干探测[36-37]以及基于空气等离子光偏置的宽带太赫兹平衡探测[38]等。近年来，基于电光采样的太赫兹波形单发探测技术已见报道[39]。光谱编码方案用线性啁啾脉冲将太赫兹时间信息映射到不同的频率上（以实现单发测量），时间分辨率受啁啾激光探测脉冲频谱分辨率的限制[40-41]；而通过引入一束未经展宽的较短激光脉冲，在两脉冲之间引入一定的时间延时，光谱仪就可探测到二者的干涉谱，时间分辨率由未经展宽的激光脉冲宽度决定，克服了时间分辨率不高的问题[42-44]。但是，光谱编码方案的整个时间窗口限制在几皮秒内，这将导致探测到的太赫兹脉冲的光谱分辨率不高。基于透射式双阶梯镜的空间编码方案将探测光的时间信息编码到探测光强的空间分布上（以实现单发测量）[45]，容易受到阶梯镜材料均匀性和光学啁啾等因素的影响。利用单个反射式金属阶梯镜将时间信息映射到镜像上的空间位置，可以减小太赫兹波形在时间上的失真[46-47]。

针对大型激光装置高能量、低重复频率泵浦的破坏性、非平衡瞬态过程的测量，笔者采用单个反射式阶梯镜与正交探测相结合的方案，设计并搭建了强场光泵浦-太赫兹波形单发探测系统。该系统具备强激光驱动下的太赫兹发射波形探测、强激光（400 nm 和 800 nm）泵浦-太赫兹波形单发探测能力。用直径为 3 inch（1 inch=2.54 cm）的铌酸锂晶片通过光整流产生太赫兹脉冲，在 1 J 激光脉冲能量驱动下产生的太赫兹脉冲能量达到了 7 μJ，太赫兹脉冲与泵浦光共线传播，光路调节方便，能够探测到 30 nm 厚自支撑金膜在室温下的透射太赫兹光谱。共线光泵浦-太赫兹波形单发探测系统分为太赫兹产生与强激光泵浦模块和太赫兹波形单发探测模块，两者分别集成到两块面包板上，前者放置于真空腔体内，后者放置于大气环境中，移动便捷，安装简单，可适应不同的激光装置使用场景。基于此系统，笔者验证了太赫兹波形单发探测能力，并在 0.8 MJ/kg 的 400 nm 激光能量密度泵浦下，获得了 30 nm 自支撑金膜在太赫兹波段的时间分辨的电导率数据，为建立准确的温稠密物质的理论模型提供了校验基准。

2 光泵浦-太赫兹单发探测系统

2.1 系统搭建

实验是在中国工程物理研究院激光聚变研究中心等离子体物理重点实验室的 45 TW Ti：sapphire 飞秒激光系统上完成的。激光系统的脉冲能量约为 1 J，中心波长为 800 nm，脉冲宽度为 25 fs，光斑直径为 38 mm。搭建的光泵浦-太赫兹波形单发探测系统如图 1 所示。图 1（a）展示了整个系统的结构示意图，800 nm 激光导入到光路中，首先经过磷酸二氢钾（KDP，尺寸为 55 mm×55 mm×3 m）晶体进行倍频，然后通过镀膜双色镜（DM）实现基频光与倍频光的分离。经双色镜透射的基频光经分束镜（BS）分束，其反射的 90% 能量作为厚度为 1 mm、直径为 3 inch 的铌酸锂晶片的驱动光，利用共线光整流效应产生强的太赫兹脉冲。在铌酸锂晶片后放置塑料片和硅片，将透过铌酸锂的激光挡掉。用金属镜（MM）调节太赫兹脉冲的方向后利用离轴抛物面反射镜（OAP）进行聚焦。随后进行太赫兹脉冲的收集与准直，将太赫兹引导进入最后一个 OAP 进行聚焦，并利用氧化铟锡导电薄膜（ITO）反射使太赫兹聚焦于电光探测晶体碲化锌（ZnTe，厚度 1.5 mm）表面。透射 10% 的飞秒激光能量作为探测光经延迟线 TD1 后，以 14°入射角入射反射式阶梯镜（RE），将时间信息编码到一维空间；出射激光由焦距为 175 mm 的透镜聚焦，之后经由线偏振片起偏后透过 ITO 与太赫兹在 ZnTe 晶体表面时空重合；透过 ZnTe 的探测光再经过四分之一波片后经由一个焦距为 100 mm 的透镜后成像到高速相机上。在透镜与相机之间放置了一个线偏振片 W2，其与偏振片 W1 互相垂直，两个线偏振片和四分之一波片组成了正交探测系统。两个线偏振片的消光比均达到了 10^5，但 ZnTe 晶体和四分之一波片插入后，消光比会减小到 300 左右，这是由应力引起的双折射和 ZnTe 晶体的散射导致的。

倍频光作为泵浦激光被反射进入到延迟线 TD2，经透镜聚焦后在焦前（直径约为 2 mm，略大于太赫兹焦斑直径，以保证均匀泵浦）打在靶上。在搭建过程中，将太赫兹产生与泵浦光路集成到一个圆形面包板上，将单发太赫兹探测光路集成到矩形面包板上，两者可独立安装。若将系统中的倍频晶体取出，将双色镜换成 800 nm 激光分束镜，该系统亦可利用 800 nm 泵浦-太赫兹探测研究不同的物理过程。本次实验所用皆为 400 nm 泵浦-太赫兹探测。

在光泵浦-太赫兹探测实验中使用的是厚度为 30 nm、直径为 2 mm 的自支撑金膜。图 1（b）、（c）分别展示了利用 800 nm 激光作为光源对金膜进行反射与透射成像的结果，结果显示金膜表面质量较好。图 1（d）详细展示了光泵浦-太赫兹探测的空间分布，泵浦光斜入射，太赫兹正入射。

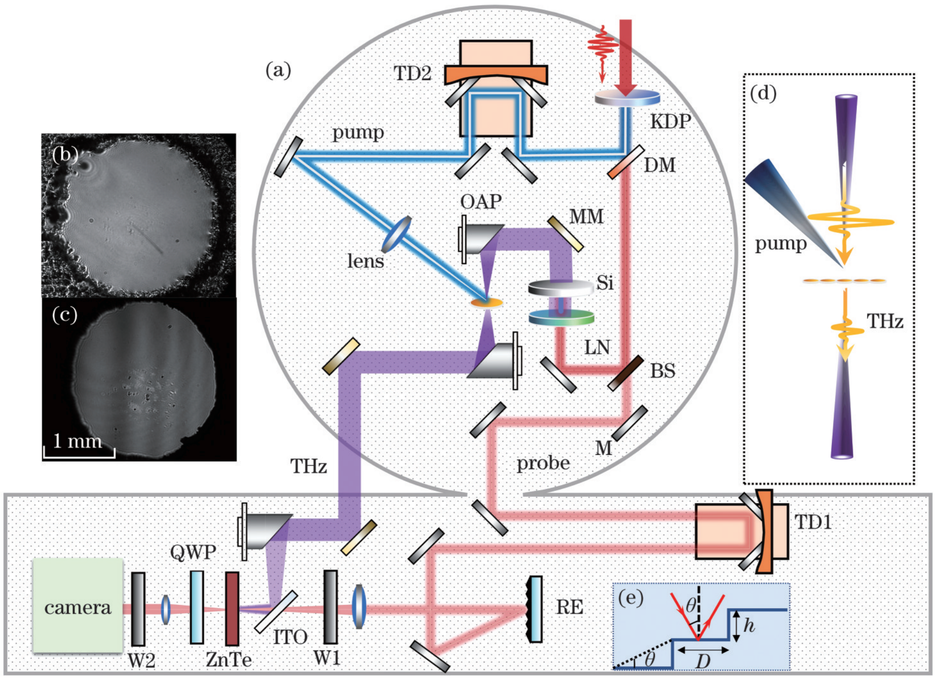

图 1　单发光泵浦-太赫兹探测系统示意图。(a)装置示意图(KDP:磷酸二氢钾;DM:双色镜;BS:激光分束镜;LN:铌酸锂晶片;OAP:离轴抛物面反射镜;MM:金属反射镜;TD1、TD2:太赫兹探测延迟线和激光泵浦延迟线;RE:反射式阶梯镜;W1、W2:线栅;ITO:氧化铟锡薄膜;ZnTe:碲化锌晶体;QWP:四分之一波片);(b)(c)直径为 2 mm、厚度为 30 nm 的自支撑金膜的反射和透射成像结果;(d)光泵浦-太赫兹探测空间布局;(e)反射式阶梯镜表面结构示意图

Fig. 1　Schematic diagrams of single-shot optical pump-terahertz detection system. (a) A schematic illustration of the setup (KDP: KH_2PO_4; DM: dichroic mirror; BS: beam splitter; LN: lithium niobate wafer; OAP: off-axis parabolic mirror; MM: metal mirror; TD1, TD2: terahertz detection delay line and pump delay line; RE: reflective echelon; W1, W2: wire grid polarizers; ITO: indium tin oxide thin film; ZnTe: zinc telluride detector crystal; QWP: 1/4 wave plate); (b)(c) reflection and transmission imaging results of free-standing gold foils with the diameter of 2 mm and the thickness of 30 nm, respectively; (d) spatial arrangement of optical pump and terahertz probe; (e) schematic diagram of the surface structure of the reflective echelon

2.2　太赫兹时域波形单发探测

在太赫兹单发探测中使用的是单个反射式阶梯反射镜，将探测光的时间信息编码到空间中，如图 1(e)所示。设探测光入射方向与阶梯水平面法线的夹角为 θ，阶梯宽度为 D，阶梯高度为 h，$\tan\theta=h/D$，则相邻阶梯之间的时间延迟为

$$\Delta t=\frac{2h}{c\cdot\cos\theta},\tag{1}$$

式中：c 为真空中的光速。来自各个阶梯的镜面反射将平面探测光斑分为 N 个(阶梯数)不同时间延迟的子光斑，相邻子光斑之间的时间延迟为 Δt。在实验中，反射式阶梯镜由国内公司定制，$h=5\ \mu m$，$D=20\ \mu m$，共 1010 个阶梯。由此计算可得时间分辨率 $\Delta t=$ 34.4 fs，探测时间窗口约为 30 ps。

太赫兹时域波形的单发探测结果与传统多发扫描结果对比如图 2 所示。图 2(a)、(b)分别为 CCD 相机记录的有太赫兹脉冲(THz on)、无太赫兹脉冲(THz off)时的探测光光强分布，图 2(c)是太赫兹调制深度 γ。调制深度 γ 的计算公式为

$$\gamma=\frac{\Delta I}{I_0}=\frac{I_{THz\,on}-I_{THz\,off}}{I_{THz\,off}},\tag{2}$$

式中：$I_{THz,on}$ 表示有太赫兹脉冲时相机测量的被调制的探测光强度；$I_{THz,off}$ 表示无太赫兹脉冲时相机测量的无调制的探测光背景强度信号。图 2(c)横轴上的像素点代表时间信息，每一行像素点都表示一个太赫兹波形。为了避免光斑不均匀带来的影响，将图 2(c)中的列像素光强值相加，得到图 2(d)所示的单发探测太赫兹波形(实线)。其中，时间轴的标定是通过改变太赫兹-探测光之间的延迟线[图 1(a)中 TD1]，记录太赫兹电场峰值的移动得到的。相邻像素点之间的时间延迟为 29.5 fs，在实验中使用此时间标度。图 2(d)中的点划线表示传统多发扫描方式测得的太赫兹波形。将两者进行归一化后再进行比较，可以发现在太赫兹主脉冲部分，单发波形和扫描波形高度重合，而在主峰之后的由空气中的水蒸气导致的振荡峰处，单发探测的太赫兹电场强度高于传统扫描得到的波形。

3　强太赫兹共线产生与表征

当铌酸锂晶片光轴与泵浦光偏振平行时，利用 Golay cell 测量太赫兹能量，得到了 5 组不同激光能量下泵浦铌酸锂晶片产生的太赫兹辐射能量与激光装置光栅对位置的依赖关系，如图 3(a)右轴所示，单个太

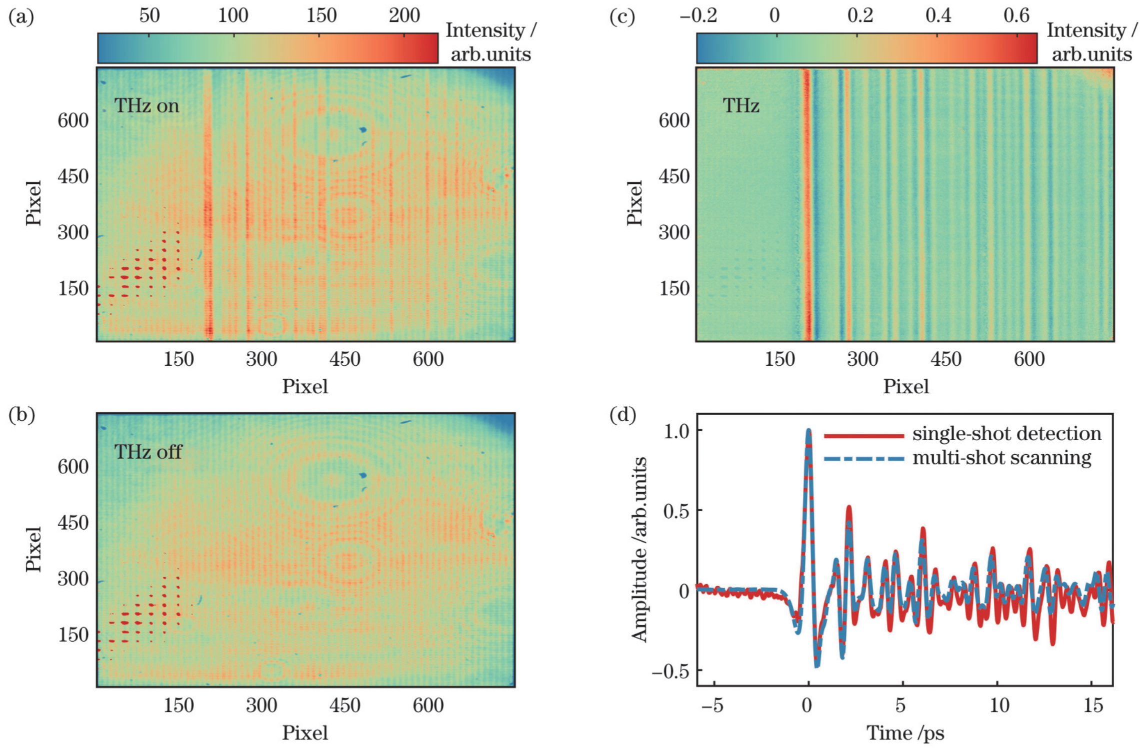

图2 单发探测与传统多发扫描探测的太赫兹波形对比。(a)有太赫兹的单发信号;(b)无太赫兹的单发背景信号;(c)单发太赫兹调制信号,$\Delta I/I_0=(I_{\mathrm{THz\,on}}-I_{\mathrm{THz\,off}})/I_{\mathrm{THz\,off}}$;(d)由(c)纵向积分得到的单发波形($\Delta I/I_0$)和传统多发扫描波形的对比,其中的实线表示单发探测结果,点划线表示传统的多点扫描结果

Fig. 2 Comparison of terahertz waveform between single-shot detection and traditional multi-shot scanning detection. (a) Single-shot signal with THz on; (b) single-shot background signal with THz off; (c) single-shot terahertz modulation signal, $\Delta I/I_0=(I_{\mathrm{THz\,on}}-I_{\mathrm{THz\,off}})/I_{\mathrm{THz\,off}}$; (d) comparison between the single-shot waveform (solid line, $\Delta I/I_0$) obtained by vertical integration of Fig. 2 (c) and the multi-shot waveform obtained by traditional multi-shot scanning (dot dash line)

赫兹脉冲能量最大达到7 μJ。图3(a)左轴表示不同光栅位置对应的激光脉宽,位置的正负表示啁啾的相对正负。可以发现:随着泵浦能量的增加,太赫兹发射对应的最优脉宽相应增大,且啁啾正负对太赫兹脉冲能量的影响并不十分明显。

同时,测量了最大泵浦脉冲能量(1 J)、最优脉宽($\tau=126$ fs)下产生的太赫兹脉冲能量通量随泵浦光强的变化,如图3(b)左轴所示。经过拟合发现,太赫兹能量通量与光强呈平方关系。计算了太赫兹能量转换效率,如图3(b)右轴所示。经过拟合后发现转换效率随光强增大呈线性增大的趋势,最大转换效率约为7×10^{-6}。这些结果说明在0.8 TW/cm^{2}光强以下,太赫兹的产生机制仍以光整流为主导。

4 温稠密金太赫兹波段电导率测量

当400 nm泵浦能量密度约为0.8 MJ/kg时,测得了不同泵浦延时下30 nm厚自支撑金膜的透射太赫兹波形,同时测量了相对应的金膜蒸发后透过小孔[图1(b)、(c)中支撑金膜的2 mm的小孔]的太赫兹波形。图4展示了泵浦探测延时为3 ps时透过金膜与小孔的太赫兹波形数据。其中,泵浦探测延时零点的标定是用硅片完成的。将0.5 mm厚的硅片放置在金膜位置,用400 nm激光泵浦产生载流子,观察到太赫兹波透过率迅速下降,将此时的泵浦探测延时标定为零延时,泵浦光与太赫兹脉冲在靶处时空重合。负延时表示太赫兹脉冲先于泵浦光到达金膜。

图4(a)、(b)分别是CCD相机记录下的透过金膜和小孔的太赫兹调制光强。利用有太赫兹和无太赫兹信号(截掉CCD相机记录的坏点部分)差分得到太赫兹调制信号,$\Delta I=I_{\mathrm{THz\,on}}-I_{\mathrm{THz\,off}}$。对其分段纵向积分,每100行积分后平均,得到$\Delta I/I_0$的太赫兹时域波形[如图4(c)、(d)所示],对其进行傅里叶变换后得到相应的频谱信息,如图4(e)、(f)所示。为了避免信号过饱和,透过小孔的太赫兹调制信号是用太赫兹线栅衰减后(衰减为原来的1/10)测得的,因此在处理时域波形[如图4(d)所示]时要乘以10。从频谱数据来看,由于太赫兹波形单发探测系统放置于大气环境中,存在水蒸气的吸收峰,会干扰频域透过率的数据分析。

为了减小探测过程中由激光器脉冲能量抖动导致的基线偏移对数据的影响,利用太赫兹时域波形的峰峰值来计算金膜的透过率。图5中的红色圆圈数据点(对应右轴)展示了太赫兹透过率随泵浦光延时的变化。

由于太赫兹波长远大于金膜厚度($\lambda\gg d=30$ nm),因此可以通过式(3)将金膜太赫兹透过率与电导率实

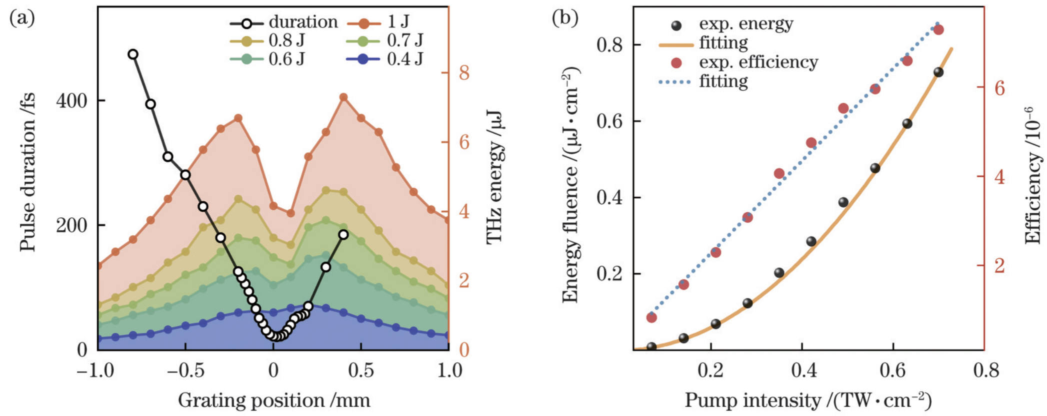

图3　太赫兹能量表征。(a)激光脉宽与光栅对位置的依赖关系，以及不同泵浦激光能量下(从上至下激光能量分别为1、0.8、0.7、0.6、0.4 J)太赫兹脉冲能量随光栅对位置的变化；(b)脉宽为126 fs时，太赫兹能量通量、转换效率随泵浦光强的变化

Fig. 3　Terahertz energy characterization. (a) The dependence of laser pulse duration on the grating position, and the variation of terahertz pulse energy with grating position for different pump laser energies (from top to bottom: 1, 0.8, 0.7, 0.6, and 0.4 J); (b) at a pulse duration of 126 fs, the terahertz energy fluence and conversion efficiency as a function of pump laser intensity

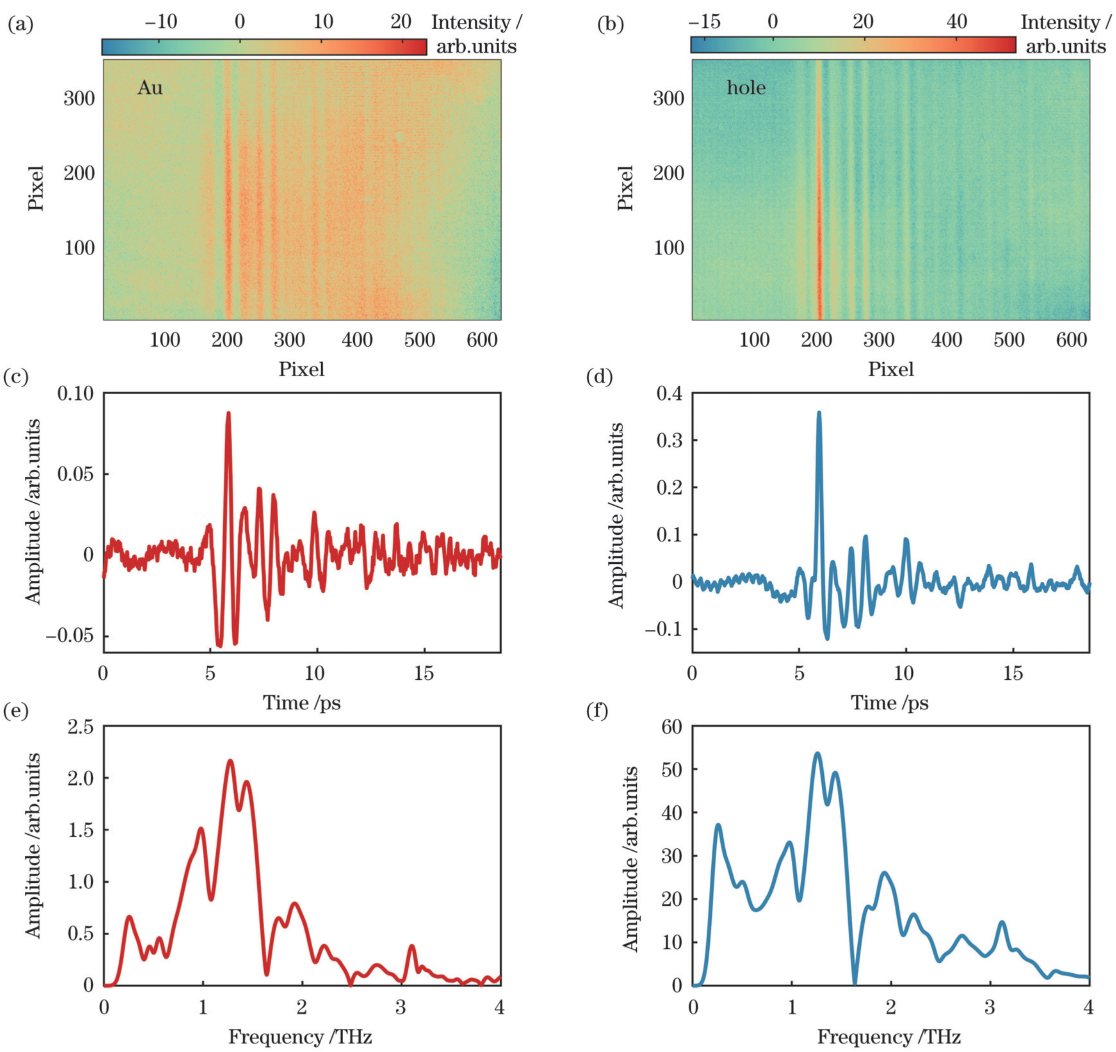

图4　泵浦延时为3 ps时金膜和小孔的太赫兹透射信号。(a)(b)金膜和小孔在有无太赫兹时探测光强的改变 $\Delta I=I_{\mathrm{THz\,on}}-I_{\mathrm{THz\,off}}$；(c)(d)由 $\Delta I/I_0$ 得到的金膜和小孔的太赫兹时域波形；(e)(f)是对应于(c)(d)的频谱

Fig. 4　Transmitted terahertz signal of the free-standing gold foil and the hole at the pump delay of 3 ps. (a)(b) Changes in probe optical intensity ($\Delta I=I_{\mathrm{THz\,on}}-I_{\mathrm{THz\,off}}$) with and without THz radiation for the gold foil and the hole, respectively; (c)(d) THz time-domain waveforms obtained from $\Delta I/I_0$ for the gold foil and the hole, respectively; (e)(f) the corresponding frequency spectra of Figs. 4(c) and (d)

部联系起来[48]。

$$|T_r|=\frac{|E_{Au}|}{|E_{Hole}|}=\left|\frac{2}{\sigma Z_0 d+2}\right|\approx\frac{2}{|\sigma|Z_0 d+2},\quad(3)$$

式中：σ表示电导率实部；E_{Au}和E_{Hole}分别表示透过金膜和相应小孔的太赫兹电场峰峰值；Z_0表示自由空间阻抗，$Z_0=337\ \Omega$。由式(3)计算出的电导率实部随泵浦延时的变化如图 5 中黑色球形数据所示(对应左轴)。室温下 30 nm 厚自支撑金膜的电导率$\sigma_0=(3.4\sim3.7)\times10^7$ S/m，与块体纯金的直流电导率数据(如图 5 中的五角星所示)接近[49]，$\sigma_{dc\ bulk}=4.403\times10^7$ S/m。

在 400 nm 激光泵浦下，电导率在泵浦延时 3 ps 内急剧下降到0.61×10^7 S/m，之后开始缓慢减小，最终在 46.7 ps 时下降到0.14×10^7 S/m。对从 0 ps 开始的电导率变化使用式(4)所示的双指数衰减函数进行拟合[50]。

$$\sigma_0=A\left[B\exp\left(-\frac{t}{\tau_1}\right)+(1-B)\exp\left(-\frac{t}{\tau_2}\right)\right]+C,(4)$$

式中：t是泵浦探测延时；τ_1和τ_2分别表示快慢弛豫时间；A和B分别表示幅度和快弛豫过程占整个过程的比例；C表示时间无关的偏移。经过拟合可得：$A=0.72$，$\tau_1=1.70$ ps，$\tau_2=167.42$ ps。拟合结果如图 5 中的实线所示(对应左轴)，将其与实验数据进行比较可以发现两者吻合得较好。这一拟合结果表明，在金膜加

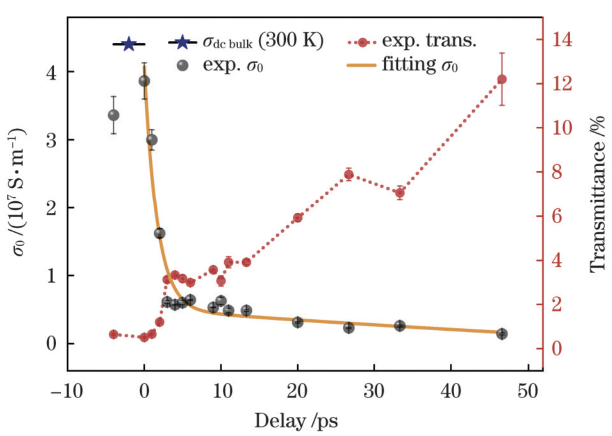

图 5 自支撑金膜电导率σ_0和太赫兹透过率随泵浦延时的变化(负延时表示太赫兹先于泵浦光到达金膜)，其中实线为双指数拟合得到的电导率随泵浦延时的变化，五角星数据点表示室温下(300 K)块体纯金的直流电导率[49]，$\sigma_{dc\ bulk}=4.403\times10^7$ S/m

Fig. 5 Variations in the electrical conductivity σ_0 and THz transmittance of the free-standing gold foil as a function of pump-probe delay (negative delay indicates that the terahertz wave arrives at the free-standing gold foil before the pump laser), where the solid line represents the time-resolved electrical conductivity at different pump-probe delay obtained from a double exponential function fit and the DC electrical conductivity of bulk pure gold at room temperature (300 K) is shown with five-pointed star symbols[49], $\sigma_{dc\ bulk}=4.403\times10^7$ S/m

热过程中，电导率的变化可能是由一个弛豫时间约为 1.7 ps 的快过程和一个较慢过程贡献的。由于金膜 5d 电子吸收 400 nm(3.1 eV)泵浦光子，电子温度在亚皮秒时间内从室温上升到 10000 K 以上，导致太赫兹透过率在最初的 3 ps 内急剧上升(电导率急剧下降)。紧接着，高温的电子系统向低温的离子系统传输能量，随着离子温度升高，太赫兹透过率缓慢上升(电导率缓慢下降)。借助双温模型，利用太赫兹透过率的跃变幅度，可以诊断激光脉冲结束后电子的温度；利用太赫兹透过率的缓慢上升，可以诊断温稠密物质电子-离子的耦合系数。

5 结　　论

太赫兹波为高能量密度物理提供了一个独特的探针。基于大型高能量密度装置产生的强场太赫兹脉冲以及太赫兹波形单发探测技术，太赫兹时域光谱技术能够诊断温稠密物质的结构和输运特性。笔者设计搭建了强激光泵浦-单发太赫兹时域光谱探测系统，并利用该系统在 45 TW 激光装置上测量了温稠密金在太赫兹波段的时间分辨的电导率，为极端非平衡物态提供了新的诊断工具。

参　考　文　献

[1] Lu J, Zhang Y Q, Hwang H Y, et al. Nonlinear two-dimensional terahertz photon echo and rotational spectroscopy in the gas phase[J]. Proceedings of the National Academy of Sciences, 2016, 113: 11800.

[2] Zhang Y Q, Shi J J, Li X, et al. Nonlinear rotational spectroscopy reveals many-body interactions in water molecules[J]. Proceedings of the National Academy of Sciences of the United States of America, 2021, 118(40): 2020941118.

[3] Hamm P, Savolainen J, Ono J, et al. Note: inverted time-ordering in two-dimensional-Raman-terahertz spectroscopy of water[J]. The Journal of Chemical Physics, 2012, 136(23): 236101.

[4] Finneran I A, Welsch R, Allodi M A, et al. Coherent two-dimensional terahertz-terahertz-Raman spectroscopy[J]. Proceedings of the National Academy of Sciences of the United States of America, 2016, 113(25): 6857-6861.

[5] Johnson C L, Knighton B E, Johnson J A. Distinguishing nonlinear terahertz excitation pathways with two-dimensional spectroscopy[J]. Physical Review Letters, 2019, 122(7): 073901.

[6] Houver S, Huber L, Savoini M, et al. 2D THz spectroscopic investigation of ballistic conduction-band electron dynamics in InSb[J]. Optics Express, 2019, 27(8): 10854-10865.

[7] Huang Y D, Xiang Z X, Xu X, et al. Localized-plasma-assisted rotational transitions in the terahertz region[J]. Physical Review A, 2021, 103(3): 033109.

[8] Ulbricht R, Hendry E, Shan J E, et al. Carrier dynamics in semiconductors studied with time-resolved terahertz spectroscopy[J]. Reviews of Modern Physics, 2011, 83(2): 543-586.

[9] Wu H Z, Guo Q A, Tu Y Y, et al. Polarity reversal of terahertz electric field from heavily p-doped silicon surfaces[J]. Chinese Physics Letters, 2021, 38(7): 074201.

[10] Chen Z, Curry C B, Zhang R, et al. Ultrafast multi-cycle terahertz measurements of the electrical conductivity in strongly excited solids[J]. Nature Communications, 2021, 12: 1638.

[11] Sie E J, Nyby C M, Pemmaraju C D, et al. An ultrafast symmetry switch in a Weyl semimetal[J]. Nature, 2019, 565(7737): 61-66.

[12] Nanni E A, Huang W R, Hong K H, et al. Terahertz-driven linear electron acceleration[J]. Nature Communications, 2015, 6: 8486.
[13] Kealhofer C, Schneider W, Ehberger D, et al. All-optical control and metrology of electron pulses[J]. Science, 2016, 352(6284): 429-433.
[14] Zhang D F, Fallahi A, Hemmer M, et al. Segmented terahertz electron accelerator and manipulator (STEAM) [J]. Nature Photonics, 2018, 12(6): 336-342.
[15] Zhang D F, Fallahi A, Hemmer M, et al. Femtosecond phase control in high-field terahertz-driven ultrafast electron sources[J]. Optica, 2019, 6(7): 872-877.
[16] Mittleman D M. Twenty years of terahertz imaging[J]. Optics Express, 2018, 26(8): 9417-9431.
[17] Chai X, Ropagnol X, Raeis-Zadeh S M, et al. Subcycle terahertz nonlinear optics[J]. Physical Review Letters, 2018, 121(14): 143901.
[18] Zalden P, Song L W, Wu X J, et al. Molecular polarizability anisotropy of liquid water revealed by terahertz-induced transient orientation[J]. Nature Communications, 2018, 9: 2142.
[19] Schubert O, Hohenleutner M, Langer F, et al. Sub-cycle control of terahertz high-harmonic generation by dynamical Bloch oscillations[J]. Nature Photonics, 2014, 8(2): 119-123.
[20] Hafez H A, Kovalev S, Deinert J C, et al. Extremely efficient terahertz high-harmonic generation in graphene by hot Dirac fermions[J]. Nature, 2018, 561(7724): 507-511.
[21] Langer F, Hohenleutner M, Schmid C P, et al. Lightwave-driven quasiparticle collisions on a subcycle timescale[J]. Nature, 2016, 533(7602): 225-229.
[22] Jelic V, Iwaszczuk K, Nguyen P H, et al. Ultrafast terahertz control of extreme tunnel currents through single atoms on a silicon surface[J]. Nature Physics, 2017, 13(6): 591-598.
[23] Schlauderer S, Lange C, Baierl S, et al. Temporal and spectral fingerprints of ultrafast all-coherent spin switching[J]. Nature, 2019, 569(7756): 383-387.
[24] Liao G Q, Li Y T, Liu H, et al. Multi millijoule coherent terahertz bursts from picosecond laser-irradiated metal foils[J]. Proceedings of the National Academy of Sciences of the United States of America, 2019, 116(10): 3994-3999.
[25] Hebling J, Stepanov A G, Almási G, et al. Tunable THz pulse generation by optical rectification of ultrashort laser pulses with tilted pulse fronts[J]. Applied Physics B, 2004, 78(5): 593-599.
[26] Jang D, Kang C, Lee S K, et al. Scalable terahertz generation by large-area optical rectification at 80 TW laser power[J]. Optics Letters, 2019, 44(22): 5634-5637.
[27] Stepanov A G, Henin S, Petit Y, et al. Mobile source of high-energy single-cycle terahertz pulses[J]. Applied Physics B, 2010, 101(1): 11-14.
[28] Hirori H, Doi A, Blanchard F, et al. Single-cycle terahertz pulses with amplitudes exceeding 1 MV/cm generated by optical rectification in $LiNbO_3$[J]. Applied Physics Letters, 2011, 98(9): 091106.
[29] Wu X J, Carbajo S, Ravi K, et al. Terahertz generation in lithium niobate driven by Ti: sapphire laser pulses and its limitations[J]. Optics Letters, 2014, 39(18): 5403-5406.
[30] Zhong S C, Li J, Zhai Z H, et al. Generation of 0.19-mJ THz pulses in $LiNbO_3$ driven by 800-nm femtosecond laser[J]. Optics Express, 2016, 24(13): 14828-14835.
[31] Wu X J, Ma J L, Zhang B L, et al. Highly efficient generation of 0.2 mJ terahertz pulses in lithium niobate at room temperature with sub-50 fs chirped Ti: sapphire laser pulses[J]. Optics Express, 2018, 26(6): 7107-7116.
[32] Zhang B L, Ma Z Z, Ma J L, et al. 1.4-mJ high energy terahertz radiation from lithium niobates[J]. Laser & Photonics Reviews, 2021, 15(3): 2000295.
[33] Wu X J, Kong D Y, Hao S B, et al. Generation of 13.9-mJ terahertz radiation from lithium niobate materials[J]. Advanced Materials, 2023, 35(23): 2208947.
[34] Auston D H, Cheung K P, Valdmanis J A, et al. Cherenkov radiation from femtosecond optical pulses in electro-optic media[J]. Physical Review Letters, 1984, 53(16): 1555-1558.
[35] Wu Q, Zhang X C. Free-space electro-optic sampling of terahertz beams[J]. Applied Physics Letters, 1995, 67(24): 3523-3525.
[36] Karpowicz N, Dai J M, Lu X F, et al. Coherent heterodyne time-domain spectrometry covering the entire "terahertz gap" [J]. Applied Physics Letters, 2008, 92(1): 011131.
[37] Dai J M, Xie X, Zhang X C. Detection of broadband terahertz waves with a laser-induced plasma in gases[J]. Physical Review Letters, 2006, 97(10): 103903.
[38] Sun X, Lü Z H, Wu H Z, et al. Broadband terahertz detection by laser plasma with balanced optical bias[J]. Sensors, 2022, 22(19): 7569.
[39] Teo S M, Ofori-Okai B K, Werley C A, et al. Invited article: single-shot THz detection techniques optimized for multidimensional THz spectroscopy[J]. Review of Scientific Instruments, 2015, 86(5): 051301.
[40] Jiang Z P, Zhang X C. Electro-optic measurement of THz field pulses with a chirped optical beam[J]. Applied Physics Letters, 1998, 72(16): 1945-1947.
[41] Kim K Y, Yellampalle B, Glownia J H, et al. Measurements of terahertz electrical conductivity of intense laser-heated dense aluminum plasmas[J]. Physical Review Letters, 2008, 100(13): 135002.
[42] van Tilborg J, Tóth C, Matlis N H, et al. Single-shot measurement of the spectral envelope of broad-bandwidth terahertz pulses from femtosecond electron bunches[J]. Optics Letters, 2008, 33(11): 1186-1188.
[43] Matlis N H, Plateau G R, van Tilborg J, et al. Single-shot spatiotemporal measurements of ultrashort THz waveforms using temporal electric-field cross correlation[J]. Journal of the Optical Society of America B, 2010, 28(1): 23-27.
[44] Li Y, Li C, Zhou M, et al. Strong terahertz radiation from relativistic laser interaction with solid density plasmas[J]. Applied Physics Letters, 2012, 100(25): 254101.
[45] Kim K Y, Yellampalle B, Taylor A J, et al. Single-shot terahertz pulse characterization via two-dimensional electro-optic imaging with dual echelons[J]. Optics Letters, 2007, 32(14): 1968-1970.
[46] Minami Y, Hayashi Y, Takeda J, et al. Single-shot measurement of a terahertz electric-field waveform using a reflective echelon mirror[J]. Applied Physics Letters, 2013, 103(5): 051103.
[47] Katayama I, Sakaibara H, Takeda J. Real-time time - frequency imaging of ultrashort laser pulses using an echelon mirror[J]. Japanese Journal of Applied Physics, 2011, 50(10R): 102701.
[48] Lloyd-Hughes J, Jeon T I. A review of the terahertz conductivity of bulk and nano-materials[J]. Journal of Infrared, Millimeter, and Terahertz Waves, 2012, 33(9): 871-925.
[49] Haynes W. CRC handbook of chemistry and physics[M]. New York: CRC Press, 2014.
[50] 才家华，张保龙，耿春艳，等. 铌酸锂强场太赫兹非线性光谱系统[J]. 中国激光，2023，50(17)：1714001.
Cai J H, Zhang B L, Geng C Y, et al. Lithium niobate strong field terahertz nonlinear spectroscopy[J]. Chinese Journal of Lasers, 2023, 50(17): 1714001.

Terahertz Time-Domain Spectroscopy of Warm Dense Gold

Sun Xu[1], Wu Haizhong[1], Wang Xiaowei[1], Lü Zhihui[1], Zhang Dongwen[1*], Liu Dongxiao[2], Fan Wei[2], Su Jingqin[2], Zhou Weimin[2], Gu Yuqiu[2], Zhao Zengxiu[1**], Yuan Jianmin[1,3***]

[1]*College of Science, National University of Defense Technology, Changsha* 410073, *Hunan, China*;

[2]*Science and Technology on Plasma Physics Laboratory, Laser Fusion Research Center, CAEP, Mianyang* 621900, *Sichuan, China*;

[3]*Graduate School of China Academy of Engineering Physics, Beijing* 100193, *China*

Abstract

Objective Terahertz (THz) waves offer a distinctive diagnostic method for detecting high energy density matter. However, realizing the THz time-domain spectral (THz-TDS) diagnosis of matter states under extreme conditions in large high-energy density devices remains a significant obstacle. To address this requirement, we designed and implemented an optical pump-THz single-shot detection system driven by a strong femtosecond laser. The system possesses the capability of THz single-shot detection under extreme conditions and diagnosis of irreversible processes with extreme transience using THz-TDS diagnosis under intense laser pumping.

Methods We developed an integrated optically pumped terahertz (THz) single-shot detection system that utilizes a 45 TW Ti:sapphire femtosecond laser with a pulse width of 30 fs, central wavelength of 800 nm, and spot diameter of approximately 38 mm. The laser pulses were initially directed to realize second harmonic generation (SHG) via KDP crystals and then separated into fundamental and SHG using a dichroic mirror (DM). The SHG was reflected into the pump time-delay line (TD2) and focused by a lens to ensure complete pumping of the target object with a focus size of approximately 2 mm in diameter consistent with the THz focus size. Meanwhile, the fundamental frequency laser transmitted by the DM was divided by the beam splitting mirror (BS) with 90% of the energy used as the driving laser of the lithium niobate wafer. An intense THz pulse was generated by collinear optical rectification effect, and an off-axis parabolic mirror (OAP) was utilized to focus it onto the target object. The THz pulses transmitted through the target object were focused by the OAP and reflected by indium tin oxide (ITO) to reach the surface of the ZnTe crystal. Moreover, 10% of the transmitted energy of the THz probe laser was directed into the time-delay line (TD1) incident with the surface normal of the reflective echelon at 14° and encoded time information into a one-dimensional space. The outgoing laser was spatiotemporal coincident with the THz on the surface of the ZnTe crystal. Finally, the orthogonal detection scheme was utilized to probe the THz waveform.

Results and Discussions We present the design and implementation of an intense-field optical pump-THz time-domain spectroscopy single-shot detection system for measuring the irreversible non-equilibrium transient processes in high-energy and low-repetition-rate pumps of large laser devices. The system employs a reflective echelon and orthogonal detection scheme to detect pulses generated through the collinear optical rectification of a lithium niobate wafer with a diameter of 3 inch. The system consists of a THz generation-intense laser pumping module and a THz time-domain spectral single-shot detection module integrated into separate optical breadboards. The former can be placed in a vacuum chamber, and the latter in an atmospheric environment, making it easy to move and install and suitable for different laser-device application scenarios. The THz pulses have an energy of 7 μJ at 800 nm 1 J laser energy, can be easily adjusted, and have a detection capability of a 30 nm free-standing gold foils transmission spectrum at room temperature. We verify that the waveform obtained by the single-shot detection is the same as that obtained by traditional scanning. Based on this device, the variation of conductivity in the THz band of 30 nm free-standing gold foils with pumping delay measured under the 0.8 MJ/kg laser energy density of a 400 nm pump contributes to the further understanding of the generation and evolution of the warm dense state of gold.

Conclusions With the advent of intense femtosecond lasers, it has become possible to investigate the state of matter in extreme conditions. The maturation of THz time-domain spectroscopy technology also provides a new tool for diagnosing extreme non-equilibrium states. To meet the demands of THz emission and state diagnosis under such extreme conditions, an intense-field optical pump-THz time-domain spectroscopy single-shot detection system with a simple THz path was designed and fabricated. The system was employed to measure the transient THz conductivity of 30 nm thick free-standing gold foils pumped by a 400 nm laser pulse. The obtained results serve as a potent platform for further exploration of irreversible processes including extreme condition THz emission-detection and the diagnosis of non-equilibrium states of matter under extreme conditions.

Key words ultrafast optics; terahertz time-domain spectroscopy; single-shot pump-probe; matter state diagnosis under extreme conditions; conductivity